

Dzyaloshinskii-Moriya interaction and the magnetic ground state in magnetoelectric LiCoPO₄Ellen Fogh,^{1,*} Oksana Zaharko,² Jürg Schefer,² Christof Niedermayer,² Sonja Holm-Dahlin,^{2,3} Michael Korning Sørensen,¹ Andreas Bott Kristensen,¹ Niels Hessel Andersen,¹ David Vaknin,⁴ Niels Bech Christensen,¹ and Rasmus Toft-Petersen¹¹*Department of Physics, Technical University of Denmark, DK-2800 Kongens Lyngby, Denmark*²*Laboratory for Neutron Scattering and Imaging, Paul Scherrer Institute, Villigen CH-5232, Switzerland*³*Nano-Science Center, Niels Bohr Institute, University of Copenhagen, DK-2100 Copenhagen Ø, Denmark*⁴*Ames Laboratory and Department of Physics and Astronomy, Iowa State University, Ames, Iowa 50011, USA*

(Received 19 November 2018; revised manuscript received 8 March 2019; published 20 March 2019)

Magnetic structures are investigated by means of neutron diffraction to shine a light on the intricate details that are believed to be key to understanding the magnetoelectric effect in LiCoPO₄. At zero field, a spontaneous spin canting of $\varphi = 7(1)^\circ$ is found. The spins tilt away from the easy b -axis toward c . Symmetry considerations lead to the magnetic point group m'_z , which is consistent with the previously observed magnetoelectric tensor form and weak ferromagnetic moment along b . For magnetic fields applied along a , the induced ferromagnetic moment couples via the Dzyaloshinskii-Moriya interaction to yield an additional field-induced spin canting. An upper limit to the size of the interaction is estimated from the canting angle.

DOI: [10.1103/PhysRevB.99.104421](https://doi.org/10.1103/PhysRevB.99.104421)**I. INTRODUCTION**

In a number of insulators, an external electric or magnetic field can induce a finite magnetization or electric polarization respectively. This so-called magnetoelectric (ME) effect was first theoretically predicted [1,2] and shortly thereafter experimentally observed in Cr₂O₃ [3,4]. Since then, a collection of materials displaying the ME effect has been identified, but the underlying microscopic mechanisms are not yet fully understood.

The Dzyaloshinskii-Moriya (DM) interaction has proved a key ingredient in explaining the induced or spontaneous electric polarization in a number of compounds such as RMnO₃ ($R = \text{Gd, Tb, Dy}$) [5], Ni₃V₂O₈ [6], and CuFeO₂ [7]. In these systems, the noncollinear incommensurate order of the magnetic moments results in a displacement of the oxygen ions situated in between neighboring moments, and a net displacement of charge is generated [8]. Noncollinear order may appear as a consequence of competing interactions, so-called spin frustration. Such systems are associated with large ME effects [8,9].

The lithium orthophosphate family (space group $Pnma$), LiMPO₄ ($M = \text{Co, Ni, Mn, Fe}$), is in many ways an excellent model system for studying the ME effect. All family members exhibit commensurate near-collinear antiferromagnetic order as well as the ME effect in their low-temperature and low-field ground state. In recent studies, additional ME phases were found at elevated magnetic fields applied along the respective easy axes in LiNiPO₄ [10] and LiCoPO₄ [11]. In both materials, these high-field ME phases are also accompanied by commensurate antiferromagnetic order [10,12].

The magnetically induced linear ME coupling is described as $P_i = \alpha_{ij}H_j$, where P_i is the electric polarization, H_j is the external magnetic field, and α_{ij} are the ME tensor

elements with $i, j = \{a, b, c\}$. Allowed tensor elements are dictated by the magnetic symmetry of the system. For collinear (anti)ferromagnets, one may think of tensor elements for which the magnetic field is *perpendicular* to the spin orientation, α_{\perp} , and those for which the field is *parallel* to the spins, α_{\parallel} . Magnitudes and temperature dependencies for α_{\perp} and α_{\parallel} have been computed from first principles for ME compounds such as Cr₂O₃ [13–16] and LiFePO₄ [17]. In these studies it is possible to separate effects due to ion displacements within the unit cell (lattice contribution) and effects due to electronic motion around “clamped” ions (electronic contribution). In both cases, one distinguishes between spin and orbital effects.

The *ab initio* calculations show that α_{\perp} is generally dominated by the spin-lattice contribution, and the ME coupling is relativistic in origin, e.g., via the DM interaction. The predicted temperature dependence of α_{\perp} follows that of the order parameter [15,17]. This corresponds well with observations in the lithium orthophosphate family except for a slight variation in the curve for LiNiPO₄ (see Fig. 1).

The behavior of α_{\parallel} is altogether more tricky, and *ab initio* calculations indicate that orbital contributions may play an important role [15,17]. When disregarding orbital contributions, the computed temperature dependence of α_{\parallel} displays a maximum below the transition temperature and then goes to zero for $T \rightarrow 0$ [14]. The comparison of the measured and predicted temperature dependencies of α_{\parallel} for LiMnPO₄ is excellent (see Fig. 1). However, for the remaining family members, $\alpha_{\parallel} \neq 0$ for $T \rightarrow 0$ and the prediction is clearly lacking. It is even worse in the case of Cr₂O₃ (not shown), where α_{\parallel} changes sign as a function of temperature [18]. The orbital moment is almost entirely quenched for LiMnPO₄ but not for LiFePO₄, LiCoPO₄, and LiNiPO₄. Hence, the discrepancy between the predicted and measured values of α_{\parallel} for $T \rightarrow 0$ for the latter three compounds may be related to the orbital moment. Moreover, the maximum magnitude of the observed ME tensor elements also appears linked to the orbital moment with $\Delta g/g = 0$ and $|\alpha_{\max}| = 0.8$ ps/m for LiMnPO₄

*elfogh@fysik.dtu.dk

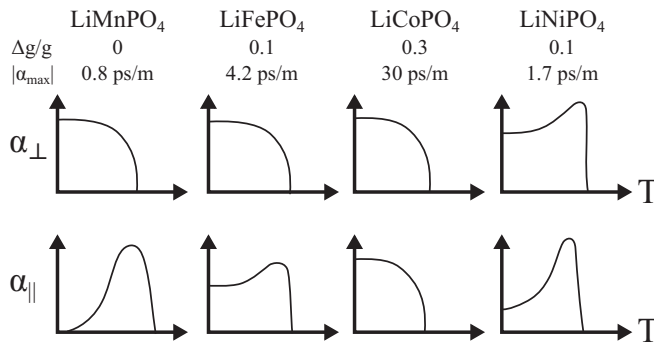


FIG. 1. Schematic of temperature dependencies of the ME tensor elements, α_{\perp} and α_{\parallel} , for the lithium orthophosphates as measured by Mercier [19]. Values of $\Delta g/g$ [20] are listed for each compound as well as maximum absolute values of the ME coefficients [21,22].

and $\Delta g/g = 0.3$ and $|\alpha_{\max}| = 30$ ps/m for LiCoPO_4 . However, recent first-principles calculations on LiFePO_4 taking into account orbital contributions (both lattice and electronic parts) still fail to encapsulate the low-temperature behavior of α_{\parallel} [17].

In this paper, we focus on LiCoPO_4 , which has by far the strongest ME effect in the lithium orthophosphate family [19,22]. Although intensively studied, there is as of yet no satisfactory theory for the underlying microscopic mechanism. LiCoPO_4 has lattice parameters $a = 10.20$ Å, $b = 5.92$ Å, and $c = 4.70$ Å [23], and the four magnetic Co^{2+} ions ($S = \frac{3}{2}$) of the crystallographic unit cell form an almost face-centered structure with the positions $\mathbf{r}_1 = (1/4 + \varepsilon, 1/4, 1 - \delta)$, $\mathbf{r}_2 = (3/4 + \varepsilon, 1/4, 1/2 + \delta)$, $\mathbf{r}_3 = (3/4 - \varepsilon, 3/4, \delta)$, and $\mathbf{r}_4 = (1/4 - \varepsilon, 3/4, 1/2 - \delta)$ and with the displacements $\varepsilon = 0.0286$ and $\delta = 0.0207$ [24]. The zero-field commensurate antiferromagnetic structure of LiCoPO_4 has spins along b (easy axis) and the four magnetic ions in a $C = (\uparrow\uparrow\downarrow\downarrow)$ arrangement [25]. Here \uparrow/\downarrow denotes spin up/down for ions on site number 1–4. The transition temperature is $T_N = 21.6$ K [26,27] and the saturation field is ~ 28 T with saturated moment $3.6\mu_B/\text{ion}$ [28]. A number of studies establish that the magnetic point group of the zero-field magnetic structure is $2'_x$ rather than mmm' as previously believed [25]. This is based on the observation of a weak ferromagnetic moment [21,29], the symmetry of the susceptibility tensor of optical second-harmonic generation [30,38], and the discovery of a toroidal moment [9,27,31–33]. The magnetic phase diagram of LiCoPO_4 was previously characterized up to 25.9 T applied along b by magnetization measurements, neutron diffraction, and electric polarization measurements [12,28,34]. At 11.9 T, the commensurate low-field structure gives way to an elliptic spin cycloid propagating along b with a period of thrice the crystallographic unit cell. The magnetic moments are in the (b, c) plane with the major axis along b . In the field interval 20.5–21.0 T, the magnetic unit cell size remains but the spins reorient. Above 21.0 T, there is a reentrance of commensurate magnetic order accompanied by the ME effect.

In this work, we investigate the possible role of spin-orbit coupling in explaining the ME effect in LiCoPO_4 as well as its sister compounds. To do so, we look into the details of

the zero-field magnetic structure of LiCoPO_4 and study the effects of a magnetic field applied along a by means of neutron diffraction and magnetometry. A spontaneous canting of spins away from the b -axis toward c is revealed. The resulting structure has magnetic point group m'_2 , and we discuss the implications related to the ME tensor form and with regard to previous studies. To investigate the DM interaction in LiCoPO_4 , we perform a neutron diffraction experiment with magnetic fields applied along a , i.e., perpendicular to the easy axis. The induced ferromagnetic moment couples via the DM interaction to yield a field-induced spin canting. We estimate the size of the DM interaction and discuss how this interaction may play a part as a generator of the ME effect in LiCoPO_4 .

II. EXPERIMENTAL DETAILS

Vibrating sample magnetization measurements were performed with a standard CRYOGENIC cryogen free measurement system. Magnetic fields of 0–16 T were applied along a for temperatures in the interval 2–300 K.

The zero-field magnetic structure was determined at the TriCS diffractometer at the Paul Scherrer Institute (PSI) employing an Euler cradle, a closed-cycle He refrigerator, open collimation, and a Ge(311) monochromator with wavelength $\lambda = 1.18$ Å. No $\lambda/2$ contamination of the beam is possible due to the diamond structure of Ge. A total of 193 inequivalent peaks were collected at 30 and 5 K.

Canting components of the zero-field structure could not be unambiguously determined at TriCS due to extinction effects and the large absorption cross section of Co. Instead, these components were investigated at the triple-axis spectrometer RITA-II at the PSI where a low background is obtained by energy discrimination. The instrument was operated in elastic mode with incoming and outgoing wavelength $\lambda = 4$ Å. A PG(002) monochromator and 80' collimation between monochromator and sample were used, and a liquid-nitrogen-cooled Be filter after the sample ensured removal of $\lambda/2$ neutrons. A cryomagnet supplied vertical magnetic fields up to 12.2 T along a and b for samples oriented with scattering planes $(0, K, L)$ and $(H, 0, L)$, respectively.

A high-quality LiCoPO_4 single crystal measuring $2 \times 2 \times 5$ mm³ (~ 20 mg) was used for magnetization measurements with magnetic fields applied along a and for neutron diffraction experiments in zero field and with magnetic fields applied along b . A second sample with dimensions $3 \times 4 \times 4$ mm³ (~ 40 mg) was used for the neutron diffraction experiment performed with fields applied along a .

III. RESULTS AND DISCUSSION

The atomic and magnetic structures of LiCoPO_4 were determined by combining data from the TriCS and RITA-II experiments. Based on the $Pnma$ space group and 241 Bragg peaks, atomic displacements of $\varepsilon = 0.028$ and $\delta = 0.020$ were refined in FULLPROF [35] ($R_F = 11.9\%$) in fair agreement with the literature [24]. The zero-field magnetic structure was determined from 130 Bragg peaks and is mainly of C_2 symmetry ($R_F = 17.2\%$), a result conforming with earlier findings [25,27]. The refined magnetic moment is $3.54(5)\mu_B$, consistent with previous magnetization measurements [28].

TABLE I. Atomic positions for LiCoPO₄ obtained from FULLPROF refinement ($R_F = 11.9\%$) using 241 Bragg peaks collected at TriCS at (30 K, 0 T) and using the $Pnma$ space group. The Debye-Waller factor was fixed to $B_{\text{iso}} = 0.20$. The magnetic moment in units of μ_B as refined using a C_y symmetry component is given in the rightmost column. This results from refinement ($R_F = 17.2\%$) using 130 commensurate magnetic peaks collected at (2 K, 0 T). The lattice parameters used in the refinements were $a = 10.20$ Å, $b = 5.92$ Å, and $c = 4.70$ Å as given in Ref. [23].

Atom	Site	x	y	z	R_y
Li	4a	0	0	0	
Co	4c	0.278(2)	0.25	0.980(3)	3.54(5)
P	4c	0.0945(8)	0.25	0.419(2)	
O1	4c	0.0986(7)	0.25	0.743(2)	
O2	4c	0.4545(7)	0.25	0.203(1)	
O3	8d	0.1669(5)	0.0463(7)	0.2826(9)	

Note that the Li occupancy was refined to 1.03(5) and hence the sample is stoichiometric within the precision of the experiment. Refinement results with the Li occupancy fixed to unity are listed in Table I.

Other magnetic structures including a minor spin rotation toward c (C_z) or a spin canting toward c (A_z) were proposed, but these refinements were not sufficiently different to distinguish them from the one regarding only a C_y component. Extinction effects and the large neutron absorption cross section of cobalt result in significantly different intensities for equivalent Bragg peaks, and hence the TriCS data only enabled identification of the major symmetry component, C_y .

Minor spin components in zero field and for magnetic fields applied along b and a were investigated at RITA-II by measuring a few key Bragg peaks: (3, 0, 1), (0, 1, 0), (1, 0, 0), (0, 2, 1), (0, 1, 2), and (0, 0, 1). Of these, only (0, 1, 0) has zero magnetic intensity. The calculated magnetic structure factors for the four basis vectors, $|S_R(\mathbf{Q})|^2$, $R = \{A, G, C, F\}$, and spin polarization factors, $|P_i(\mathbf{Q})|^2$, $i = \{x, y, z\}$, for these peaks are listed in Table II.

TABLE II. Absolute squares of structure and polarization factors for the magnetic basis vectors reflected by the key Bragg peaks used to establish the magnetic structure of LiCoPO₄. The factors are normalized to unit spin lengths. Note that the crystallographic directions a , b , and c may be used interchangeably with x , y , and z , respectively.

(H, K, L)	$ S_R(\mathbf{Q}) ^2$				$ P_i(\mathbf{Q}) ^2$		
	A	G	C	F	x	y	z
	($\uparrow\downarrow\uparrow\uparrow$)	($\uparrow\downarrow\uparrow\downarrow$)	($\uparrow\uparrow\downarrow\downarrow$)	($\uparrow\uparrow\uparrow\uparrow$)	a	b	c
(3,0,1)	0.07	0.22	11.73	3.98	0.34	1	0.66
(0,1,0)	0	0	16	0	1	0	1
(1,0,0)	15.51	0.49	0	0	0	1	1
(0,2,1)	0	15.71	0.29	0	1	0.28	0.72
(0,1,2)	0	1.14	14.86	0	1	0.86	0.14
(0,0,1)	0	15.71	0.29	0	1	1	0

The magnetic neutron intensity may then be expressed as

$$I(\mathbf{Q}) \propto S^2 f(\mathbf{Q})^2 \sum_R |S_R(\mathbf{Q})|^2 \sum_i |P_i(\mathbf{Q})|^2, \quad (1)$$

where $f(\mathbf{Q})$ is the magnetic form factor and S is the thermal average of the magnetic moment. The following analysis is based on a process of eliminating possible structures and is not a full structure refinement.

A. Spontaneous spin canting at zero field

In addition to the major C_y spin component, a smaller symmetry component was identified by observation of magnetic intensity at the (1,0,0) position. This peak mainly represents magnetic structures of A symmetry with spins polarized along either b or c . It is approximately one order of magnitude weaker than (3,0,1) [compare Figs. 2(a) and 2(b)], which may be assumed to represent the major spin component when regarding the following argument: both (3,0,1) and (0,1,0) appear if a C component is present, but the two peaks represent different spin polarizations. (3,0,1) is present for any spin orientation, whereas (0,1,0) is only present for components along a or c . Since (0,1,0) has no magnetic intensity [see Fig. 2(c)] we can exclude those two spin directions entirely. Hence, the (3,0,1) magnetic Bragg peak may be assumed to solely represent a C_y spin arrangement.

Next, the basis vector corresponding to the (1,0,0) Bragg peak is identified. The thermal average of the spin is most often maximized at low temperatures. Since an A -type component with spins along b would produce spins of varying lengths, it is therefore reasonable to assume that the observed magnetic intensity at (1,0,0) is instead due to a spin component along c . The result is a canting of the spins in the (b, c) plane, and the canting angle, φ , is estimated by comparing the intensity of (1,0,0) with that of (3,0,1). Following the above arguments, it is assumed that (3,0,1) represents only a C_y symmetry component, and (1,0,0) represents only an A_z component such that the measured intensities may be written as in Eq. (1),

$$I_{(1,0,0)} \propto |S_A^{(1,0,0)}|^2 |P_z^{(1,0,0)}|^2 f_{(1,0,0)}^2,$$

$$I_{(3,0,1)} \propto |S_C^{(3,0,1)}|^2 |P_b^{(3,0,1)}|^2 f_{(3,0,1)}^2.$$

The spontaneous canting angle is then calculated from the corrected intensities, $I_{(1,0,0)}^{\text{corr}}$ and $I_{(3,0,1)}^{\text{corr}}$, as $\tan \varphi = \sqrt{I_{(1,0,0)}^{\text{corr}}/I_{(3,0,1)}^{\text{corr}}}$. The usual Lorentz factor for two-axis diffractometers, $\sin(2\theta)$, is also taken into account, and although not entirely correct for the triple-axis setup [36], the correction is estimated to introduce an error of at most 10% for the two implicated Bragg peaks. The calculated angle is shown in Fig. 2(e) where both data at 0 and 10 T along b are shown. The canting angle is temperature-independent below the transition temperature and it is also independent of the applied magnetic field. The magnetic structure is thus locked in with a spontaneous canting angle of $\varphi = 7(1)^\circ$ as estimated from a weighed mean of all data points in Fig. 2(e). The resulting zero-field structure is illustrated in Fig. 3(a). Note that the (3,0,1) Bragg peak is relatively strong compared to (1,0,0) and is therefore, to a larger extent, subject to extinction effects. Consequently, the calculated angle may be overestimated.

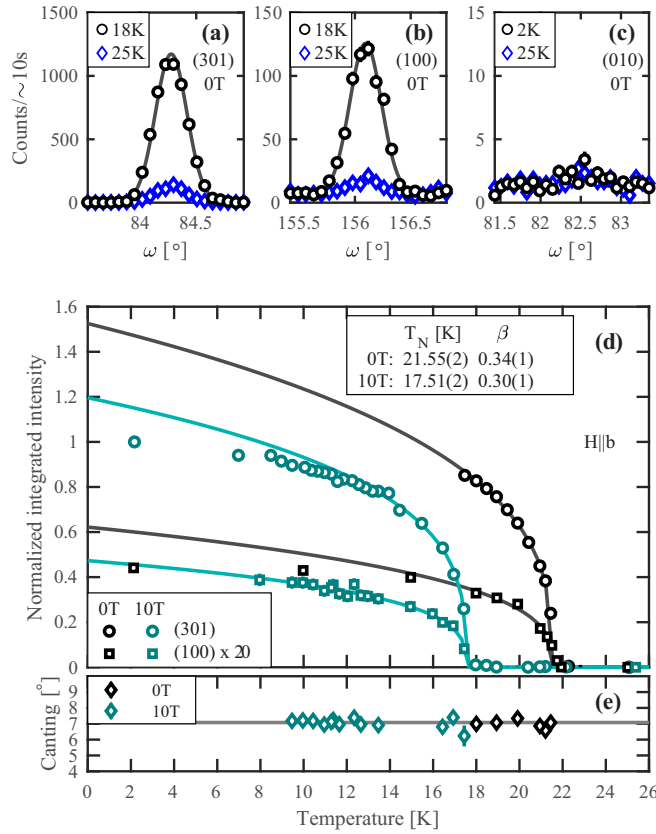


FIG. 2. Neutron diffraction data from RITA-II. (a)–(c) Rocking curves of (3, 0, 1), (1, 0, 0), and (0, 1, 0) at 18 or 2 K (black circles) and 25 K (blue diamonds), all at 0 T. The solid lines are Gaussian fits from which the integrated intensities are obtained. The canting angle of the zero-field structure is estimated from the intensity ratio between the magnetic contributions of (3, 0, 1) and (1, 0, 0). (d) Integrated magnetic intensity of (3, 0, 1) (circles) and (1, 0, 0) (squares) as a function of temperature at 0 T (black symbols) and 10 T along b (green symbols). The intensities have been normalized to the value of (3, 0, 1) at the lowest temperature, and the intensity of (1, 0, 0) has been multiplied by 20 for a better comparison of the temperature profiles. Backgrounds at 25 K have been subtracted. The solid lines show fits to a power law, $I \propto (T - T_N)^\beta$, for $T > 17$ K at 0 T and $T > 13$ K at 10 T. The transition temperature, T_N , and critical exponent, β , were fitted collectively for the two peaks. (e) Spontaneous canting angle calculated from the intensity ratio of (1, 0, 0) and (3, 0, 1) for measurements done at 0 T (black symbols) and 10 T (green symbols). The horizontal line shows the value of the weighted mean of all data points, $\varphi = 7(1)^\circ$.

Both (3, 0, 1) and (1, 0, 0) appear at the same transition temperature—see Fig. 2(d)—and therefore reflect the same order parameter. Indeed, a power law with a collectively fitted transition temperature, $T_N = 21.55(2)$ K, and a critical exponent, $\beta = 0.34(1)$, describe the recorded data well. However, note that the C -type structure polarized along b and the A -type structure polarized along b or c are not contained within the same irreducible representation of the lithium orthophosphates; see Table III.

The Bragg peaks (0, 2, 1), (0, 1, 2), and (0, 0, 1) also have magnetic intensity at 0 T. These peaks are all present for a C_y structure but may also represent a G -type component

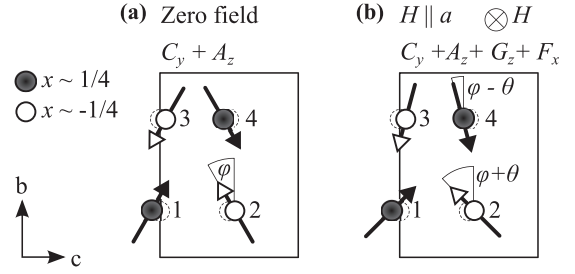


FIG. 3. Projections in the (b , c) plane of the magnetic structures of LiCoPO_4 at (a) zero field and for (b) $H \parallel a$. For clarity, only the four magnetic ions of the unit cell are shown and all angles are largely exaggerated. The ion positions deviate slightly from the high-symmetry positions (dashed circles). The applied field yields asymmetric total canting angles.

polarized along either a or b ; see Table II. A G_y component is unlikely due to maximized moments at low temperatures and is not compatible with the observed ME effect, toroidal moment, and weak ferromagnetism. Furthermore, G_x is paired with F_z in the irreducible representations, see Table III, and F_z is not present [29]. Therefore, the magnetic intensity at the (0, 2, 1), (0, 1, 2), and (0, 0, 1) positions at 0 T may be subscribed to the major C_y spin component.

It is commented that the determined zero-field structure does not fully agree with earlier findings. A C_z -type rotation of the spins away from the b -axis was reported in Ref. [27] based on the observation of the (0, 1, 0) magnetic peak. However, as seen in Fig. 2(c), we observe zero magnetic intensity at the (0, 1, 0) position. A maximum of the rotation angle of $0.7(3)^\circ$ is estimated from the error on the measured zero intensity. This is contrasted by the 4.6° reported in Ref. [27]. One possible explanation for the discrepancy might be found in slightly different levels of Li in different samples. Previously, changes in atomic bond lengths and magnetic properties of Li_zCoPO_4 with $z = 0.2, 0.7$ as compared to the stoichiometric compound, LiCoPO_4 , were reported [37]. It is conceivable that small variations in Li content between samples may bring about small differences in the exact magnetic structure. As already mentioned, our sample was found to have a Li occupancy of 1.03(5).

It has been repeatedly suggested [27, 30, 38] that the zero-field structure of LiCoPO_4 has lower symmetry than the originally proposed magnetic point group mmm' [25]. The observed 4.6° rotation of spins restricts symmetry to $2'_x/m_x$, which is further reduced to $2'_x$ when requiring a weak ferromagnetic component along b . Indeed, optical second-harmonic generation measurements advocate that the

TABLE III. Irreducible representations, magnetic space groups, and corresponding basis vectors for $Pnma$.

Γ_1	Γ_2	Γ_3	Γ_4	Γ_5	Γ_6	Γ_7	Γ_8
$Pnma$	$Pnm'a'$	$Pn'ma'$	$Pn'm'a'$	$Pn'm'a'$	$Pn'ma$	$Pnm'a$	$Pnma'$
	F_x		G_x	C_x		A_x	
G_y		F_y			A_y		C_y
	G_z		F_z	A_z		C_z	

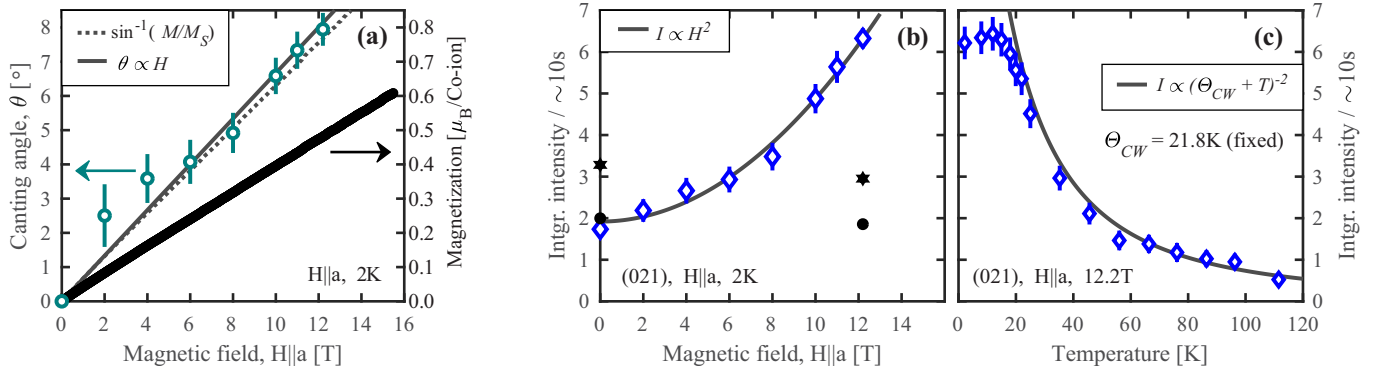


FIG. 4. Magnetization, field-induced canting angle, and integrated neutron intensity of (0,2,1) for magnetic fields applied along a . (a) Magnetization (thick black line) and field-induced canting angle (green circles) calculated from the neutron intensity of (0,2,1) as a function of applied field. Both are to a good approximation linearly proportional to the field strength. The solid line shows a linear fit to the canting angle, whereas the dashed line shows the angle as calculated from the magnetization with $M_s = 3.6\mu_B/\text{ion}$. (b) and (c) Integrated intensity (blue diamonds) of (0,2,1) as a function of applied field at 2 K and as a function of temperature at 12.2 T, respectively. The field dependence in (b) and the temperature dependence in (c) have been fitted to a quadratic and a Curie-Weiss law squared, respectively (solid lines). The black symbols in (b) show intensities for (0,1,2) (circles) and (0,0,1) (stars) at 0 and 12.2 T. Note that the intensities for these peaks are scaled to appear together with the intensity of (0,2,1) in order to demonstrate that they show no or only little field dependence.

point-group symmetry is $2'_x$ [38]. This point group allows for a toroidal moment [39] and the linear ME effect with tensor elements $\alpha_{ab}, \alpha_{ba} \neq 0$ [40], consistent with measurements [21]. In addition, $2'_x$ allows the tensor elements $\alpha_{ac}, \alpha_{ca} \neq 0$, which are not measurably different from zero [21], but the spin rotation angle introduces only a small deviation from mmm' . Furthermore, as the point group merely yields the *allowed* ME tensor elements, they are not *necessarily* active.

Thus neutron diffraction [27], SQUID [41], and optical second-harmonic generation measurements [30,38] all paint a picture of LiCoPO_4 having magnetic point group $2'_x$ in its zero-field state. In contrast, our observation of a spontaneous spin canting rather than a rotation leads to the magnetic point group $2_z/m'_z$. This point group also allows for a toroidal moment and the ME tensor elements $\alpha_{aa}, \alpha_{ab}, \alpha_{ba}, \alpha_{bb}, \alpha_{cc} \neq 0$ where only the off-diagonal elements are measurably different from zero. Again, we note that the canting angle only presents a small deviation from mmm' . $2_z/m'_z$ does not support a ferromagnetic moment along b rendering it inconsistent with observations. However, removing the twofold axis enables a ferromagnetic moment in the (a, b) plane. Thus, the magnetic point group m'_z is consistent with our neutron diffraction data and a weak ferromagnetic moment along b . Note, however, that it is not consistent with the observed optical second-harmonic generation signal [30,38].

Interestingly, m'_z is also consistent with the previous neutron diffraction study when using a different—but still correct—interpretation of the presented data. The rotation of the spins toward c was established based on observation of the (0,1,0) magnetic Bragg peak. However, this rotation might equally well be toward a . Assuming such a rotation results in magnetic point group $2_z/m'_z$, which again needs relaxing to m'_z to allow for a ferromagnetic moment along b . In addition, the C_x component belongs to the same irreducible representation as the A_z component (see Table III) and as is deduced in the next section; the two components combined yield a favorable energy term via the DM interaction. Therefore, our observations may in fact be consistent with the previous studies,

and the magnetic point group of the zero-field structure of LiCoPO_4 is m'_z .

B. Field-induced spin canting for $H \parallel a$

For magnetic fields applied along a , LiCoPO_4 is linearly magnetized with the field as seen in the magnetization data in Fig. 4(a). A ferromagnetic contribution to the spin structure is induced with $S^a = \alpha H$ and fitted slope $\alpha = 0.0395(1)\mu_B/\text{T}$. Furthermore, yet another antiferromagnetic component exists in addition to the established main structure of C_y symmetry and the minor A_z component. This extra component is manifested by an increase in the intensity of the (0,2,1) magnetic Bragg peak as a function of applied field; see Fig. 4(b). The magnetic origin of the (0,2,1) intensity is confirmed by its temperature dependence that follows a Curie-Weiss law squared; see Fig. 4(c).

The (0,2,1) peak represents mainly spin arrangements of symmetry G and to a smaller extent structures of symmetry C ; cf. Table II. All spin orientations are possible, and more information is therefore needed in order to pin down which magnetic structure the additional intensity of (0,2,1) signifies. Again, the argument follows a process of elimination using two other magnetic Bragg peaks: (0,1,2) and (0,0,1).

The (0,1,2) peak is present for any C spin structures. This peak has no additional field-induced intensity [see Fig. 4(b)], and consequently any additional C spin elements are ruled out. Finally, (0,0,1) represents G symmetry with spins polarized along a or b . Again, this peak shows no change upon applying a magnetic field along a [see Fig. 4(b)], and these magnetic structure types may also be rejected. The only remaining possible magnetic structure as a contributor to the (0,2,1) field-induced intensity is then G_z . This component comes as an addition to the already established major C_y component and the smaller A_z component. An asymmetry is introduced in the canting angles such that spins (1,2) and (3,4) form pairs with canting angles $\varphi + \theta$ and $\varphi - \theta$, respectively. Here $\theta \equiv \theta(H)$ is the field-induced canting angle. The resulting magnetic

structure for magnetic fields applied along a is shown in Fig. 3(b).

The size of θ is now estimated. As previously argued, it may be assumed that at 0 T, (0, 2, 1) only reflects the C_y structure. Any additional intensity upon applying a field then originates from the G_z component:

$$I_{(0,2,1)}(H) - I_{(0,2,1)}(0 \text{ T}) \propto |S_G^{(0,2,1)}|^2 |P_z^{(0,2,1)}|^2.$$

This is to be compared to the intensity of (0,2,1) at 0 T:

$$I_{(0,2,1)}(0 \text{ T}) \propto |S_C^{(0,2,1)}|^2 |P_y^{(0,2,1)}|^2.$$

Since only one peak is involved in the determination of the field-induced canting angle, there is no need to correct for the magnetic form factor or Lorentz factor, and any extinction or absorption effects may be neglected. The field-induced canting angle is then calculated as $\tan \theta = \sqrt{\frac{I_{(0,2,1)}^{\text{corr}}(H) - I_{(0,2,1)}^{\text{corr}}(0 \text{ T})}{I_{(0,2,1)}^{\text{corr}}(0 \text{ T})}}$ and is to a good approximation linear as a function of applied field along a : $\theta = \beta H$ with fitted slope $\beta = 0.012(1)$ rad/T [see Fig. 4(a)]. The field-induced canting angle as deduced from the magnetization, $\sin \theta = M/M_S$, is also shown in Fig. 4(a) and substantiates the link between F_x and G_z . Furthermore, since the neutron intensity is proportional to the ordered magnetic moment squared, a linear coupling between the ferromagnetic moment and the canted moment would result in a quadratic increase in the neutron intensity of (0,2,1) as a function of applied field. This is indeed the case, as shown in Fig. 4(b). Here the solid line is a fit to a quadratic dependence, $I \propto H^2$. The measured intensity is clearly well described by the fit. Additionally, the symmetry elements G_z and F_x belong to the same irreducible representation; see Table III.

C. Dzyaloshinskii-Moriya interaction

An estimate of the size of the DM interaction in LiCoPO₄ may be obtained from the field-induced spin canting. A similar calculation was previously performed for the sister compound LiNiPO₄, and the analysis in Ref. [42] is directly applicable here. Symmetry arguments lead to the only allowed DM coefficients $\mathbf{D}_{14} = (0, D_{14}^b, 0) = -\mathbf{D}_{23}$ and $\mathbf{D}_{12} = (0, D_{12}^b, 0) = \mathbf{D}_{34}$. These yield terms in the Hamiltonian of the form

$$\begin{aligned} \mathcal{H}_{\text{DM}}^1 &= \mathbf{D}_{14} \cdot (\mathbf{S}_1 \times \mathbf{S}_4) - \mathbf{D}_{14} \cdot (\mathbf{S}_2 \times \mathbf{S}_3) \\ &= D_{14}^b (S_1^c S_4^a - S_1^a S_4^c - S_2^c S_3^a + S_2^a S_3^c) \quad \text{and} \\ \mathcal{H}_{\text{DM}}^2 &= \mathbf{D}_{12} \cdot (\mathbf{S}_1 \times \mathbf{S}_2) + \mathbf{D}_{12} \cdot (\mathbf{S}_3 \times \mathbf{S}_4) \\ &= D_{12}^b (S_1^c S_2^a - S_1^a S_2^c + S_3^c S_4^a - S_3^a S_4^c). \end{aligned}$$

The spin component along a is finite for $H \parallel a$ and assumed equal at all sites, i.e., $S_1^a = S_2^a = S_3^a = S_4^a = S^a > 0$. In this case, both terms favor a G_z -type order, and this is exactly what we observe. The ferromagnetic moment along a therefore induces—via the DM interaction—an antiferromagnetic spin component of symmetry G_z .

The field-induced G_z component leaves the nearest-neighbor spin pairs (1,4) and (2,3) antiparallel, and hence no energy change is to be expected from the term $\mathcal{H}_{\text{DM}}^1$ nor from the nearest-neighbor exchange term. On the other hand, the term $\mathcal{H}_{\text{DM}}^2$ does indeed yield a finite energy contribution for

a G_z component. The strength of the DM interaction may be estimated by balancing the different energy contributions for spins deviating from the easy axis, b :

$$\left. \begin{aligned} \mathcal{H}_{\text{DM}} &= 4D_{12}^b S^a S \sin \theta \\ \mathcal{H}_{\text{ani}} &= 4\mathcal{D}^c S^2 \sin^2 \theta \end{aligned} \right\} \Rightarrow \frac{D_{12}^b}{\mathcal{D}^c} = \frac{-S \sin \theta}{S^a} \approx -S \frac{\theta}{S^a},$$

where \mathcal{D}^c is the single-ion anisotropy constant for spin components along c , $S = 3.6\mu_B$ is the saturated moment, $\sin \theta \approx \theta$ holds for small canting angles, $\theta = \beta H$, and $S^a = \alpha H$. With the fitted coefficients $\beta = 0.012(1)$ rad/T and $\alpha = 0.0395(1) \mu_B/\text{T}$, the ratio becomes $D_{12}^b/\mathcal{D}^c \approx -1.1$. Note that this is an upper bound for the size of the DM interaction as the above simple calculation neglects any competing exchange interactions, which may also influence the spin canting.

Thus, the DM interaction in LiCoPO₄ may be as large as the single-ion anisotropy along c . The full spin Hamiltonian of LiCoPO₄ has not been determined yet, but limited inelastic neutron scattering data show an almost dispersionless spin excitation along the (0, K , 0) direction, and a single-ion anisotropy constant of $\mathcal{D}^c \approx 0.7$ meV is suggested [27,43,44]. This is a very strong DM interaction, and its possible role as a generator for the ME effect in LiCoPO₄ is discussed in the following.

Magnetostrictive mechanisms successfully explain the ME effect in LiNiPO₄ [10,42] and LiFePO₄ [20] based on magnetic-field-induced changes in the exchange and DM interactions, respectively. A similar model would be expected to describe the effect in LiCoPO₄. However, so far a satisfactory model has eluded all our efforts—both when considering magnetic-field-induced changes in the exchange and DM interactions individually and combined. Such microscopic models inherently result in a ME coefficient, α_{\parallel} , proportional to $\chi_{\parallel}(S)^2$, i.e., the magnetic susceptibility and the order parameter. The susceptibility drops at low temperatures in a collinear antiferromagnet, and the order parameter levels out after the initial increase at the transition. Hence the temperature dependence of α_{\parallel} has a maximum below the transition as seen in LiMnPO₄, LiNiPO₄, and LiFePO₄ (revisit Fig. 1). However, for LiCoPO₄, α_{\parallel} does not display such a maximum as a function of temperature. In fact, its temperature profile resembles that of the order parameter, and the curves are similar for α_{\parallel} and α_{\perp} .

As discussed in the Introduction, it was previously proposed that the spin-orbit coupling is a central element in fully understanding the ME effect in the lithium orthophosphates. However, *ab initio* calculations considering both spin and orbital momentum on an equal footing still fail to correctly predict the size of α_{\parallel} for $T \rightarrow 0$ in LiFePO₄ [17]. The spin-orbit coupling is expected to be larger in the sister compound, LiCoPO₄, and similar first-principles computations may be expected to produce larger ME coefficients. To the best of our knowledge, such calculations have yet to be performed. Nevertheless, our neutron diffraction data show that there is indeed a large DM interaction in LiCoPO₄ that in turn relates to the spin-orbit coupling. Therefore, it remains that the spin-orbit coupling plays an important role in generating the ME effect in LiCoPO₄—and most likely in the entire family of compounds. This emphasizes the need for more

theoretical work and improved *ab initio* calculations in order to elucidate the missing mechanism(s) governing the linear ME effect in LiCoPO₄, and even better to explain the link between the spin-orbit coupling and the ME effect in the lithium orthophosphates in general. Moreover, spin excitation measurements would enable modeling of the spin Hamiltonian of LiCoPO₄ and thereby provide a better understanding of the magnetic interactions in the system.

IV. CONCLUSIONS

Intricate details of the zero-field magnetic structure of LiCoPO₄ were investigated in the hope of illuminating the microscopic mechanism behind the large magnetoelectric effect in LiCoPO₄. The Co²⁺ ions mainly order in a commensurate antiferromagnetic structure of C_y symmetry. Additionally, we discover a spontaneous spin canting of $\varphi = 7(1)^\circ$ originating in an A_z spin component. The resulting zero-field magnetic structure belongs to the magnetic point group m'_z , consistent with previously reported experimental results.

For magnetic fields applied along *a*, a second minor spin component of symmetry G_z is induced. The canting angle increases to a good approximation linearly with the applied field and is shown to be induced via the Dzyaloshinskii-Moriya interaction by the ferromagnetic moment along *a*. The upper limit for the size of the Dzyaloshinskii-Moriya interaction was estimated to be approximately equal to that of the single-ion anisotropy constant along *c*. This shows that the spin-orbit coupling is strong in LiCoPO₄, and we discuss how it may be linked to its large magnetoelectric effect.

ACKNOWLEDGMENTS

This work was supported by the Danish Agency for Science and Higher Education under DANSCATT. Neutron diffraction experiments were performed at the Swiss spallation neutron source SINQ, Paul Scherrer Institute, Villigen, Switzerland. Ames Laboratory is operated by the U.S. Department of Energy by Iowa State University under Contract No. DE-AC02-07CH11358.

-
- [1] L. D. Landau and E. M. Lifshitz, *Electrodynamics of Continuous Media* (Pergamon, Oxford, UK, 1960).
- [2] I. E. Dzyaloshinskii, On the magneto-electrical effect in antiferromagnets, *J. Exp. Theor. Phys.* **10**, 628 (1960).
- [3] D. N. Astrov, The magnetoelectric effect in antiferromagnetics, *J. Exp. Theor. Phys.* **11**, 708 (1960).
- [4] D. N. Astrov, Magnetoelectric effect in chromium oxide, *J. Exp. Theor. Phys.* **13**, 729 (1961).
- [5] I. A. Sergienko and E. Dagotto, Role of the Dzyaloshinskii-Moriya interaction in multiferroic perovskites, *Phys. Rev. B* **73**, 094434 (2006).
- [6] M. Kenzelmann, A. B. Harris, A. Aharony, O. Entin-Wohlman, T. Yildirim, Q. Huang, S. Park, G. Lawes, C. Broholm, N. Rogado, R. J. Cava, K. H. Kim, G. Jorge, and A. P. Ramirez, Field dependence of magnetic ordering in kagomé-staircase compound Ni₃V₂O₈, *Phys. Rev. B* **74**, 014429 (2006).
- [7] T. Kimura, J. C. Lashley, and A. P. Ramirez, Inversion-symmetry breaking in the noncollinear magnetic phase of the triangular-lattice antiferromagnet CuFeO₂, *Phys. Rev. B* **73**, 220401 (2006).
- [8] T. Kimura, Spiral magnets as magnetoelectrics, *Annu. Rev. Mater. Res.* **37**, 387 (2007).
- [9] N. A. Spaldin, M. Fiebig, and M. Mostovoy, The toroidal moment in condensed-matter physics and its relation to the magnetoelectric effect, *J. Phys.: Condens. Matter* **20**, 434203 (2008).
- [10] R. Toft-Petersen, E. Fogh, T. Kihara, J. Jensen, K. Fritsch, J. Lee, G. E. Granroth, M. B. Stone, D. Vaknin, H. Nojiri, and N. B. Christensen, Field-induced reentrant magnetoelectric phase in LiNiPO₄, *Phys. Rev. B* **95**, 064421 (2017).
- [11] V. M. Khrustalyov, V. M. Savvitsky, and M. F. Kharchenko, Magnetoelectric effect in antiferromagnetic LiCoPO₄ in pulsed magnetic fields, *Low Temp. Phys.* **42**, 280 (2016).
- [12] E. Fogh, R. Toft-Petersen, E. Ressouche, C. Niedermayer, S. L. Holm, M. Bartkowiak, O. Prokhnenko, S. Sloth, F. W. Isaksen, D. Vaknin, and N. B. Christensen, Magnetic order, hysteresis, and phase coexistence in magnetoelectric LiCoPO₄, *Phys. Rev. B* **96**, 104420 (2017).
- [13] J. Íñiguez, First-Principles Approach to Lattice-Mediated Magnetoelectric Effects, *Phys. Rev. Lett.* **101**, 117201 (2008).
- [14] M. Mostovoy, A. Scaramucci, N. A. Spaldin, and K. T. Delaney, Temperature-Dependent Magnetoelectric Effect from First Principles, *Phys. Rev. Lett.* **105**, 087202 (2010).
- [15] A. Malashevich, S. Coh, I. Souza, and D. Vanderbilt, Full magnetoelectric response of Cr₂O₃ from first principles, *Phys. Rev. B* **86**, 094430 (2012).
- [16] S. Mu, A. L. Wysocki, and K. D. Belashchenko, First-principles microscopic model of exchange-driven magnetoelectric response with application to Cr₂O₃, *Phys. Rev. B* **89**, 174413 (2014).
- [17] A. Scaramucci, E. Bousquet, M. Fechner, M. Mostovoy, and N. A. Spaldin, Linear Magnetoelectric Effect by Orbital Magnetism, *Phys. Rev. Lett.* **109**, 197203 (2012).
- [18] G. T. Rado and V. J. Folen, Observation of The Magnetically Induced Magnetoelectric Effect and Evidence for Antiferromagnetic Domains, *Phys. Rev. Lett.* **7**, 310 (1961).
- [19] M. Mercier, Étude de l'effet magnetoelectrique sur de composés de type olivine, perovskite et grenat, Ph.D. thesis, Université de Grenoble, 1969.
- [20] R. Toft-Petersen, M. Reehuis, T. B. S. Jensen, N. H. Andersen, J. Li, M. Duc Le, M. Laver, C. Niedermayer, B. Klemke, K. Lefmann, and D. Vaknin, Anomalous magnetic structure and spin dynamics in magnetoelectric LiFePO₄, *Phys. Rev. B* **92**, 024404 (2015).
- [21] J.-P. Rivera, The linear magnetoelectric effect in LiCoPO₄ revisited, *Ferroelectrics* **161**, 147 (1994).
- [22] W. S. Wiegelhofer and A. Lakhtakia, *Introduction to Complex Mediums for Optics and Electromagnetics* (SPIE, Bellingham, Washington, USA, 2003).
- [23] R. E. Newnham and M. J. Redman, Crystallographic data for LiMgPO₄, LiCoPO₄ and LiNiPO₄, *J. Am. Ceram. Soc.* **48**, 547 (1965).

- [24] F. Kubel, Crystal structure of lithium cobalt double orthophosphate, LiCoPO_4 , *Z. Kristallogr.* **209**, 755 (1994).
- [25] R. P. Santoro, D. J. Segal, and R. E. Newnham, Magnetic properties of LiCoPO_4 and LiNiPO_4 , *J. Phys. Chem. Solids* **27**, 1192 (1966).
- [26] A. Szewczyk, M. U. Gutowska, J. Wieckowski, A. Wisniewski, R. Puzniak, R. Diduszko, Yu. Kharchenko, M. F. Kharchenko, and H. Schmid, Phase transitions in single-crystalline magneto-electric LiCoPO_4 , *Phys. Rev. B* **84**, 104419 (2011).
- [27] D. Vaknin, J. L. Zarestky, L. L. Miller, J.-P. Rivera, and H. Schmid, Weakly coupled antiferromagnetic planes in single-crystal LiCoPO_4 , *Phys. Rev. B* **65**, 224414 (2002).
- [28] N. F. Kharchenko, V. M. Khrustalev, and V. N. Savitskii, Magnetic field induced spin reorientation in the strongly anisotropic antiferromagnetic crystal LiCoPO_4 , *Low Temp. Phys.* **36**, 558 (2010).
- [29] Y. Kharchenko, N. Kharchenko, M. Baran, and R. Szymczak, *Magnetoelectric Interaction Phenomena in Crystals (MEIPIC-5)*, edited by M. Fiebig, V. V. Eremanko and I. E. Chubis (Kluwer-Academic, Dordrecht, 2004), p. 227.
- [30] B. B. Van Aken, J.-P. Rivera, H. Schmid, and M. Fiebig, Anisotropy of Antiferromagnetic 180° Domains in LiCoPO_4 and LiNiPO_4 , *Phys. Rev. Lett.* **101**, 157202 (2008).
- [31] C. Ederer and N. A. Spaldin, Towards a microscopic theory of toroidal moments in bulk periodic crystals, *Phys. Rev. B* **76**, 214404 (2007).
- [32] B. B. Van Aken, J.-P. Rivera, H. Schmid, and M. Fiebig, Observation of ferrotoroidic domains, *Nat. Lett.* **449**, 702 (2007).
- [33] A. S. Zimmermann, D. Meier, and M. Fiebig, Ferroic nature of magnetic toroidal order, *Nat. Commun.* **5**, 4796 (2014).
- [34] V. M. Khrustalyov, V. M. Savytsky, and M. F. Kharchenko, (H, T_i) -diagram of magnetic transformations induced by a pulsed magnetic field in antiferromagnetic LiCoPO_4 , *Low Temp. Phys.* **43**, 1332 (2017).
- [35] J. Rodríguez-Carvajal, Recent advances in magnetic structure determination by neutron powder diffraction, *Physica B* **192**, 55 (1993).
- [36] R. Pynn, Lorentz factors for triple-axis spectrometers, *Acta Crystallogr. B* **31**, 2555 (1975).
- [37] H. Ehrenberg, N. N. Bramnik, A. Senyshyn, and H. Fuess, Crystal and magnetic structures of electrochemically delithiated $\text{Li}_{1-x}\text{CoPO}_4$ phases, *Solid State Sci.* **11**, 18 (2009).
- [38] A. S. Zimmermann, B. B. Van Aken, H. Schmid, J.-P. Rivera, J. Li, D. Vaknin, and M. Fiebig, Anisotropy of antiferromagnetic 180° domains in magnetoelectric LiMPO_4 ($M = \text{Fe}, \text{Co}, \text{Ni}$), *Eur. Phys. J. B* **71**, 355 (2009).
- [39] H. Schmid, Some symmetry aspects of ferroics and single phase multiferroics, *J. Phys.: Condens. Matter* **20**, 434201 (2008).
- [40] J.-P. Rivera, A short review of the magnetoelectric effect and related experimental techniques on single phase (multi-) ferroics, *Eur. Phys. J. B* **71**, 299 (2009).
- [41] N. F. Kharchenko, Yu. N. Kharchenko, R. Szymczak, M. Baran, and H. Schmid, Weak ferromagnetism in the antiferromagnetic magnetoelectric crystal LiCoPO_4 , *Low Temp. Phys.* **27**, 895 (2001).
- [42] T. B. S. Jensen, N. B. Christensen, M. Kenzelmann, H. M. Rønnow, C. Niedermayer, N. H. Andersen, K. Lefmann, J. Schefer, M. Zimmermann, J. Li, J. L. Zarestky, and D. Vaknin, Field-induced magnetic phases and electric polarization in LiNiPO_4 , *Phys. Rev. B* **79**, 092412 (2009).
- [43] W. Tian, J. Li, J. W. Lynn, J. L. Zarestky, and D. Vaknin, Spin dynamics in the magnetoelectric effect compound LiCoPO_4 , *Phys. Rev. B* **78**, 184429 (2008).
- [44] We have examined crystals from the same batch as that used in Ref. [43] and find a significantly lower transition temperature, $T_N = 17.3(1)\text{K}$. Furthermore, a Rietveld refinement of our neutron diffraction data yields satisfactory results exclusively when introducing Ni as well as Co on the magnetic site. Hence, our results suggest that the crystals may not be pure LiCoPO_4 , but possibly Ni-doped from a crucible growth.